Available online at www.sciencedirect.com
SCIENCE DIRECT®
PERGAMON
International Journal of Heat and Mass Transfer 46 (2003) 2341–2351
International Journal of HEAT and MASS TRANSFER
www.elsevier.com/locate/ijhmt

Complex combination solution for radiation–conduction transport with periodic boundary conditions

Ted D. Bennett *

Department of Mechanical and Environmental Engineering, University of California, Santa Barbara, CA 93106, USA

Received 26 July 2002; received in revised form 2 December 2002

Abstract

A solution method for radiation–conduction transport is developed using complex combination. This method offers an alternative to the direct temporal integration of the transient radiation–conduction equation for problems with periodic boundary conditions, where the sustained solution is of interest. A solution is formulated as an expansion series of temperature fields having frequencies that are multiples of those imposed by the boundary conditions. This series is shown to converge rapidly for most problems, making it a very efficient technique.
© 2003 Elsevier Science Ltd. All rights reserved.

Keywords: Radiation–conduction transport; Periodic boundary conditions; Complex combination

1. Introduction

A solution method is developed for combined radiation-conduction transport in an optically gray material having periodic heating applied at the boundaries. The transient radiation–conduction equation has been solved before; for a few examples of these solutions see [1–4]. Here a quasi-steady-state solution is of interest, which exists after a time long in comparison with the period of heating. While direct time integration could be used to obtain this solution, this approach is computationally expensive. Therefore, a method using complex combination is proposed to obtain the sustained response of the material to periodic heating in the presence of both radiation and conduction transport.

A number of important problems can benefit from the complex combination method developed here. Analysis of thermal barrier coatings under the high heat loads found in modern engines is one example [5,6]. Yttria stabilized zirconia coatings used commercially as thermal barrier coatings are partially transparent to thermal radiation [7,8]. The material design of these coatings is an important area of research, in which improving the thermal performance is an important goal [9–13]. As the operational temperatures of engines continue to rise, the radiative component of the heat load applied to these coatings grows faster than the convective load. Therefore, the improved optical performance of these coatings, with respect to thermal radiation, is an important new issue. The complex combination method developed here will permit temporal analysis of thermal barrier coatings in systems such as reciprocating engines. Previous heat transfer analysis of thermal barrier coatings in diesel engines, for example, was limited to available steady techniques for mixed conduction–radiation transport [5]. With the complex combination method, a more accurate description of the transient thermal performance of these coatings can be realized.

The complex combination method is well developed for problems of diffusion by conduction [14]. However, the method has not been applied previously to mixed radiation–conduction transport because of the nonlinear nature of this problem. For diffusion by conduction

* Tel.: +1-805-893-8115; fax: +1-805-893-8651.
E-mail address: bennett@engineering.ucsb.edu (T.D. Bennett).

0017-9310/03/$ - see front matter © 2003 Elsevier Science Ltd. All rights reserved.
doi:10.1016/S0017-9310(02)00535-5

Nomenclature

a	absorption coefficient (1/m)
a_j	real tensor coefficient (Eq. (12))
$\tilde{b}_j$	complex tensor coefficient (Eq. (12))
c_j	real tensor coefficient (Eq. (12))
C	heat capacity (K/kg K)
$\tilde{d}_j$	complex tensor coefficient (Eq. (12))
E_1	dimensionless exponential integral function
E_2	dimensionless exponential integral function
I_r	total radiation intensity (W/m^2 sr)
k	thermal conductivity (W/m K)
L	plane-wall thickness (m)
$\mathbb{m}$	real part of refractive index
N	number of frequencies in expansion
Nu	Nusselt number $Nu = hL/k$
Q	dimensionless conduction flux $Q = q_c/(4\mathbb{m}^2\sigma T_r^4)$
q_c	conduction flux (W/m^2)
$\vec{q}_r$	radiation flux (W/m^2)
S	dimensionless radiation source term (Eq. (3b))
$\tilde{S}_{n\Omega}$	$n\Omega$ frequency of radiation source term (Eq. (9))
T	temperature (K)
T_r	characteristic reference temperature (K)
$\overline{T}$	steady temperature component (K)
$\tilde{T}_{n\omega}$	$n\omega$ frequency of temperature (K)
t	time (s)
x	coordinate (m)

Greek symbols

η	dimensionless coordinate $\eta = x/L$
κ	dimensionless conduction–radiation parameter $\kappa = k/(4\mathbb{m}^2\sigma T_r^3 L)$
λ	dimensionless optical thickness $\lambda = aL$
θ	dimensionless temperature $\theta = T/T_r$
$\bar{\theta}_0$	dimensionless steady temperature component
$\tilde{\theta}_{n\Omega}$	$n\Omega$ frequency of dimensionless temperature
$\tilde{\theta}^4_{n\Omega}$	$n\Omega$ frequency of θ^4
ρ	density
σ	Stefan–Boltzmann constant (5.67×10^{-8} W/m^2 K^4)
τ	dimensionless time $\tau = 4\mathbb{m}^2\sigma T_r^3 t/(\rho CL)$
Ω	dimensionless fundamental frequency $\Omega = \rho CL\omega/(4\mathbb{m}^2\sigma T_r^3)$
ω	frequency (dω unit solid angle)

Subscripts

a	front fluid
b	back fluid
J	mesh size
j	node number
$n\Omega$	frequency component

Superscript

m	iteration number

alone, with harmonic boundary conditions, the temperature solution is harmonic with the same fundamental frequency as the boundary conditions. However, by including radiation transport, emission and re-absorption of energy within the material introduces higher order frequencies into the temperature solution. For the case in which the medium is gray, the spectrally integrated emission intensity is proportional to the fourth power of temperature T^4. By virtue of this power law, the higher order frequencies can be directly express as multiples of the fundamental frequency ω. For example, the temperature described by the combination of a steady temperature $\overline{T}$ and a single frequency temperature $\tilde{T}_\omega$ causes energy to radiate into four frequencies: 1ω, 2ω, 3ω, and 4ω, through terms related to $\overline{T}^3\tilde{T}_\omega$, $\overline{T}^2\tilde{T}^2_\omega$, $\overline{T}\tilde{T}^3_\omega$ and $\tilde{T}^4_\omega$, respectively. Once these frequencies are present in the radiative field, they will appear in the temperature solution due to re-absorption of radiation within the medium. Consequently, the temperature solution for mixed conduction–radiation transport with harmonic boundary conditions will be nonharmonic. To apply complex combination, a solution for $T(\vec{x}, t)$ is sought by decomposing the temperature field into a series of fields with frequencies that are multiples of the fundamental frequency imposed by the boundary condition.

For each frequency in the expanded solution, temperature has a prescribed temporal form that allows for a complex number representation. The only unknowns are the amplitude and phase of the temperature field at each frequency. However, the solution procedure is complicated by the fact that each temperature frequency is coupled to other frequencies through the radiative term in the transport equation. Furthermore, for any finite number of temperature frequencies N, the radiative power law introduces $4N$ frequencies into the solution. Therefore, a series solution will converge only if the amplitudes of higher order temperature frequencies become small. Working in favor of this is the heat capacity of the material, which naturally lends to increased dampening as the frequency of temperature component increases.

2. Formulation

The transient radiation–conduction transport equation can be written in the form [15]

$$\rho C(\partial T/\partial t) - k\nabla^2 T + \vec{\nabla}\cdot\vec{q}_r = 0, \tag{1a}$$

$$\vec{\nabla}\cdot\vec{q}_r = a\left[4\sigma T^4 - \int_0^{4\pi} I_r \,\mathrm{d}\omega\right]. \tag{1b}$$

Transient storage of energy is related to the heat capacity of the material through the first term of Eq. (1a). The second term reflects conduction transport, and radiation transport is expressed as a spectrally integrated source in the third term. This source term is the divergence of the radiative flux expressed in Eq. (1b), and depends upon the difference between the local powers of emission and irradiant absorption. The magnitude of local irradiant absorption depends upon radiation that evolves from all other locations within the material domain and from outside the domain boundaries.

To simplify the presentation of the complex combination solution for radiation–conduction transport, a one-dimensional plane-wall problem is considered which is shown schematically in Fig. 1. Energy is transferred from a source through the front boundary and transferred to a sink through the back boundary. The fluid temperatures on either side on the plane-wall are used to specify a blackbody source and sink for radiation heat transfer. The front and back surfaces are assumed reflectionless to thermal radiation, and real part of the refractive index $\mathbb{m}$ of the fluids are matched to the plane-wall. Boundary conditions on the temperature field must also be applied to the plane-wall at each surface. The usual possibilities are to specify the temperature, conduction flux, or convection coefficient. In this work, heat is introduced by a conduction flux or specified temperature boundary condition at $x = 0$ (Eqs. (2a,b)) and removed with a convection or specified temperature boundary condition at $x = L$ (Eqs. (2c,d))

$$\mathrm{BC}(x=0): -\vec{\nabla}_x T\cdot\vec{n} = q_c(t)/k \quad \text{or} \quad T = T_a(t), \tag{2a,b}$$

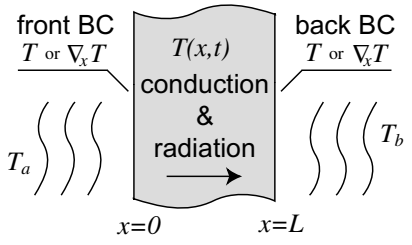

Fig. 1. One-dimensional plane-wall problem schematically showing radiative fluids and boundary conditions considered. The front and back surfaces are reflectionless to thermal radiation, and real part of the refractive index $\mathbb{m}$ of the fluids are matched to the plane-wall.

$$\mathrm{BC}(x=L): -\vec{\nabla}_x T\cdot\vec{n} = (h/k)(T - T_b(t)) \quad \text{or} \quad T = T_b(t). \tag{2c,d}$$

The boundary conditions related to heat flux concern conduction heat transfer only. Radiative loading through the boundaries of the wall is reconciled in the radiative source term given by Eq. (1b).

The problem expressed by Eqs. (1) and (2) may be nondimensionalized as follows. A characteristic reference temperature of the problem is used to nondimensionalize the dependent temperature variable $\theta = T/T_r$. The independent variables for space and time are nondimensionalized as $\eta = x/L$ and $\tau = 4\mathbb{m}^2\sigma T_r^3 t/(\rho CL)$, respectively. In terms of these variables, the governing dimensionless equation for temperature in the plane-wall becomes [15]

$$\partial\theta/\partial\tau - \kappa\nabla_\eta^2\theta + \lambda S = 0, \tag{3a}$$

$$S = \theta^4(\eta) - \frac{1}{2}\left[\theta_a^4 E_2(\lambda\eta) + \theta_b^4 E_2(\lambda[1-\eta]) + \lambda\int_0^1 \theta^4(\eta')E_1(\lambda|\eta'-\eta|)\,\mathrm{d}\eta'\right]. \tag{3b}$$

Coefficients related to conduction and radiation transport appear in the nondimensional terms: $\kappa = k/(4\mathbb{m}^2\times\sigma T_r^3 L)$ and $\lambda = aL$. The conduction–radiation parameter κ reflects the importance of conduction relative to radiation transport, and λ is the optical thickness of the plane-wall. Eq. (3b) assumes a nonscattering medium, and E_1 and E_2 are exponential integral functions.

Terms in Eq. (3a) retain the same interpretation as in dimensional form. Eq. (3b) expresses the nondimensional radiant energy related to the source term, in which the leading θ^4 reflects emission. Absorption of radiation originating from outside the plane-wall is associated with the emissive powers of two bounding fluids at temperatures of θ_a and θ_b, while absorption of radiation originating from locations within the plane-wall is associated with the final integral term.

In nondimensional form, the boundary conditions given by Eqs. (2a–d) become

$$\mathrm{BC}(\eta=0): -\vec{\nabla}_\eta\theta\cdot\vec{n} = Q/\kappa \quad \text{or} \quad \theta = \theta_a, \tag{4a,b}$$

$$\mathrm{BC}(\eta=1): -\vec{\nabla}_\eta\theta\cdot\vec{n} = Nu(\theta-\theta_b) \quad \text{or} \quad \theta = \theta_b. \tag{4c,d}$$

The specified heat flux at the front boundary in nondimensional form becomes $Q = q_c/(4\mathbb{m}^2\sigma T_r^4)$. The Nusselt number $Nu = hL/k$ appears in the convection condition in Eq. (4c).

The boundary conditions impose a fundamental frequency ω on the solution. Although this analysis can be extended to allow for more than one, it is assumed here that only one fundamental frequency exists. In

nondimensional form, the fundamental frequency is $\Omega = \omega t/\tau = \rho CL\omega/(4\mathbb{n}^2\sigma T_r^3)$. A solution to the problem stated by Eqs. (3) and (4) is sought through an expansion of temperature fields having frequencies that are multiples of the fundamental frequency

$$\theta(\eta,\tau) = \bar{\theta}_0 + \tilde{\theta}_\Omega e^{i\Omega\tau} + \tilde{\theta}_{2\Omega} e^{i2\Omega\tau} + \cdots + \tilde{\theta}_{N\Omega} e^{iN\Omega\tau}. \tag{5}$$

Whenever temperature is represented by a complex number, as is the case in Eq. (5), it is implied that only the real part is taken. Notice that the coefficients $\tilde{\theta}_{n\Omega}$ ($0 \leqslant n \leqslant N$) are spatial variables only, and are complex with the exception of $n = 0$. When Eq. (5) is substituted into the governing partial differential equation (3a), the result can be organized into a system of ordinary differential equations, each equation representing one frequency of the temperature field expansion

$$\kappa\nabla_\eta^2 \begin{Bmatrix} \bar{\theta}_0 \\ \tilde{\theta}_\Omega \\ \tilde{\theta}_{2\Omega} \\ \vdots \\ \tilde{\theta}_{N\Omega} \end{Bmatrix} - i\Omega \begin{Bmatrix} 0 \\ 1\tilde{\theta}_\Omega \\ 2\tilde{\theta}_{2\Omega} \\ \vdots \\ N\tilde{\theta}_{N\Omega} \end{Bmatrix} = \lambda \begin{Bmatrix} \overline{S}_0 \\ \widetilde{S}_\Omega \\ \widetilde{S}_{2\Omega} \\ \vdots \\ \widetilde{S}_{N\Omega} \\ \vdots \\ \widetilde{S}_{4N\Omega} \end{Bmatrix} \text{truncated} \tag{6}$$

For any finite number of temperature frequencies N, radiation transfer will introduce terms with up to $4N$ times the fundamental frequency. Therefore, terms with frequencies greater than $N\Omega$ must be dropped from the system of equations to be solved (Eq. (6)). It remains to be shown that if N is chosen sufficiently large, the truncated terms are negligible.

With the exception of the first equation, the solution to each equation in Eq. (6) is a complex temperature field that contains information about the amplitude and the phase of the time varying field for one frequency. The first equation describes the steady component of the solution and therefore is real rather than complex.

One complication in setting up the system given by Eq. (6) is that the radiation term for each frequency must be calculated from the nonlinear Eq. (3b), which depends on the fourth power of the temperature field. With temperature θ expressed as the expansion given in Eq. (5), θ^2 can be expressed in an expansion of $2N$ frequencies

$$\theta^2 = \sum_{n=0}^{N}\sum_{m=n}^{N}(1-\delta_{mn}/2)[\tilde{\theta}_{m\Omega}\tilde{\theta}_{n\Omega}e^{i(m+n)\Omega t} + \tilde{\theta}^*_{n\Omega}\tilde{\theta}_{m\Omega}e^{i(m-n)\Omega t}]. \tag{7}$$

In Eq. 7, $\tilde{\theta}^*_{n\Omega}$ and $\tilde{\theta}^*_{m\Omega}$ are complex conjugates of the nth and mth frequencies in Eq. (5), and δ_{mn} is the Kronecker delta operator. Using the expression for θ^2, θ^4 can be expressed as the expansion of $4N$ frequencies

$$\theta^4 = \sum_{n=0}^{2N}\sum_{m=n}^{2N}(1-\delta_{mn}/2)[\tilde{\theta}^2_{m\Omega}\tilde{\theta}^2_{n\Omega}e^{i(m+n)\Omega t} + \tilde{\theta}^2_{m\Omega}\tilde{\theta}^{2*}_{n\Omega}e^{i(m-n)\Omega t}]. \tag{8}$$

Using Eq. 8 to identify each term $\tilde{\theta}^4_{n\Omega}$ in the expression for θ^4, the radiation term for each frequency is calculated from

$$\widetilde{S}_{n\Omega} = \tilde{\theta}^4_{n\Omega}(\eta) - \frac{1}{2}\left[\tilde{\theta}^4_{a,n\Omega}E_2(\lambda\eta) + \tilde{\theta}^4_{b,n\Omega}E_2(\lambda[1-\eta]) + \lambda\int_0^1 \tilde{\theta}^4_{n\Omega}(\eta')E_1(\lambda|\eta'-\eta|)\,d\eta'\right]. \tag{9}$$

It should be noted that $\tilde{\theta}^4_{n\Omega}$ is the nth frequency in the expansion of θ^4 and not the fourth power of the nth frequency of θ. The terms $\tilde{\theta}^4_{a,n\Omega}$ and $\tilde{\theta}^4_{b,n\Omega}$ relate to the emissive powers of the two bounding fluids and are evaluated in a similar manner to $\tilde{\theta}^4_{n\Omega}$.

To complete the problem formulation, the boundary conditions are expressed in terms of the decomposed temperature field

$$\mathrm{BC}(\eta=0): -\vec{\nabla}_\eta\tilde{\theta}_{n\Omega}\cdot\vec{n} = \widetilde{Q}_{n\Omega}/\kappa \quad \text{or} \quad \tilde{\theta}_{n\Omega} = \tilde{\theta}_{a,n\Omega}, \tag{10a,b}$$

$$\mathrm{BC}(\eta=1): -\vec{\nabla}_\eta\tilde{\theta}_{n\Omega}\cdot\vec{n} = Nu(\tilde{\theta}_{n\Omega} - \tilde{\theta}_{b,n\Omega}) \quad \text{or} \quad \tilde{\theta}_{n\Omega} = \tilde{\theta}_{b,n\Omega}. \tag{10c,d}$$

The heat flux Q and specified temperatures θ_a and θ_b must have a finite number of frequencies associated with them. Boundary conditions are harmonic if $\widetilde{Q}_\Omega$ is the highest nonzero frequency term associated with Q, and $\tilde{\theta}_{a,\Omega}$ and $\tilde{\theta}_{b,\Omega}$ are the highest nonzero frequency terms associated with the boundary fluid temperatures.

3. Method of solution

The problem is cast into a finite difference form to obtain a numerical solution. Because the governing equation is nonlinear, an iterative approach to the solution is used. Eq. (6) is written as

$$\kappa\nabla^2_\eta\tilde{\theta}^{m+1}_{n\Omega} - i\Omega n\tilde{\theta}^{m+1}_{n\Omega} = \lambda\widetilde{S}^{m+1}_{n\Omega} \tag{11}$$

to solve for the $n\Omega$ temperature component resulting from the $m+1$ iteration. Eq. (11) can be expressed in terms of the known temperature field from the mth iteration using $\tilde{\theta}^{m+1}_{n\Omega} = \tilde{\theta}^m_{n\Omega} + \Delta\tilde{\theta}^m_{n\Omega}$, and the change in temperature field at each frequency $\Delta\tilde{\theta}_{n\Omega}$ solved for. The change in the radiation term is linearly approximated by $\widetilde{S}^{m+1}_{n\Omega} \approx \widetilde{S}^m_{n\Omega} + (\widetilde{S}^m_{n\Omega}/d\tilde{\theta}_{n\Omega})\Delta\tilde{\theta}_{n\Omega}$. After being expressed in terms of the temperature change at each node, Eq. (11) is discretized by expressing the second derivative with a

central difference scheme. This yields a tridiagonal system of equations

$$\begin{bmatrix} \tilde{b}_0 & c_0 & & \\ a_1 & \ddots & \ddots & \\ & \ddots & \ddots & c_{J-2} \\ & & a_{J-1} & \tilde{b}_{J-1} \end{bmatrix} \begin{bmatrix} \Delta\tilde{\theta}_0 \\ \Delta\tilde{\theta}_1 \\ \vdots \\ \Delta\tilde{\theta}_{J-1} \end{bmatrix}^m_{n\Omega} = \begin{bmatrix} \tilde{d}_0 \\ \tilde{d}_1 \\ \vdots \\ \tilde{d}_{J-1} \end{bmatrix}^m_{n\Omega}. \quad (12)$$

For uniformly distributed nodes, the coefficients to Eq. (12) for interior nodes $1 \leqslant j \leqslant J-2$ are

$$a_j = \frac{-\kappa}{(\Delta\eta)^2}, \quad \tilde{b}_j = \frac{2\kappa}{\Delta\eta^2} + i\Omega n + \lambda \left.\frac{d\widetilde{S}^m_{n\Omega}}{d\theta_{n\Omega}}\right|_j, \quad c_j = \frac{-\kappa}{(\Delta\eta)^2} \quad (13a\text{–}c)$$

$$\tilde{d}_j = \kappa \frac{\left.\tilde{\theta}^m_{n\Omega}\right|_{j+1} - 2\left.\tilde{\theta}^m_{n\Omega}\right|_j + \left.\tilde{\theta}^m_{n\Omega}\right|_{j-1}}{(\Delta\eta)^2} - i\Omega n \left.\tilde{\theta}^m_{n\Omega}\right|_j - \lambda \left.\widetilde{S}^m_{n\Omega}\right|_j. \quad (13d)$$

For $j = 0$, the heat flux boundary condition can be implemented with

$$\tilde{b}_0 = \frac{\kappa}{\Delta\eta^2} + \frac{i\Omega n}{2} + \frac{\lambda}{2} \left.\frac{d\widetilde{S}^m_{n\Omega}}{d\theta_{n\Omega}}\right|_0, \quad c_0 = \frac{-\kappa}{(\Delta\eta)^2}, \quad (14a,b)$$

$$\tilde{d}_0 = \frac{\widetilde{Q}_{n\Omega}}{\Delta\eta} + \kappa \frac{\left.\tilde{\theta}^m_{n\Omega}\right|_1 - \left.\tilde{\theta}^m_{n\Omega}\right|_0}{(\Delta\eta)^2} - \frac{i\Omega n}{2}\left.\tilde{\theta}^m_{n\Omega}\right|_0 - \frac{\lambda}{2}\left.\widetilde{S}^m_{n\Omega}\right|_0. \quad (14c)$$

Alternatively, a specified constant temperature boundary condition can be implemented with

$$\tilde{b}_0 = 1, \quad c_0 = 0, \quad \tilde{d}_0 = \tilde{\theta}_{a,n\Omega}. \quad (15a\text{–}c)$$

For $j = J-1$, the convection boundary condition can be implemented with:

$$a_{J-1} = \frac{-\kappa}{(\Delta\eta)^2}, \quad (16a)$$

$$\tilde{b}_{J-1} = \frac{\kappa}{\Delta\eta}\left[Nu + \frac{1}{\Delta\eta}\right] + \frac{i\Omega n}{2} + \frac{\lambda}{2}\left.\frac{d\widetilde{S}^m_{n\Omega}}{d\theta_{n\Omega}}\right|_{J-1} \quad (16b)$$

$$\tilde{d}_{J-1} = \frac{\kappa}{\Delta\eta} Nu\left(\tilde{\theta}_{b,n\Omega} - \left.\tilde{\theta}^m_{n\Omega}\right|_{J-1}\right) + \kappa \frac{\left.\tilde{\theta}^m_{n\Omega}\right|_{J-2} - \left.\tilde{\theta}^m_{n\Omega}\right|_{J-1}}{(\Delta\eta)^2} - \frac{i\Omega n}{2}\left.\tilde{\theta}^m_{n\Omega}\right|_{J-1} - \frac{\lambda}{2}\left.\widetilde{S}^m_{n\Omega}\right|_{J-1}. \quad (16c)$$

Alternatively, a specified constant temperature back boundary condition can be implemented with

$$a_{J-1} = 0, \quad \tilde{b}_{J-1} = 1, \quad \tilde{d}_{J-1} = \tilde{\theta}_{b,n\Omega}. \quad (17a\text{–}c)$$

The radiation derivative term, appearing in Eqs. (13b), (14a) and (16b), is evaluated with respect to a local change in a temperature. Therefore, $(d\widetilde{S}_{n\Omega}/d\tilde{\theta}_{n\Omega}) = (d\tilde{\theta}^4_{n\Omega}/d\tilde{\theta}_{n\Omega})$, which can be evaluated from Eq. (8) as

$$\frac{d\widetilde{S}_{n\Omega}}{d\tilde{\theta}_{n\Omega}} = \sum_{m=0}^{2N} \begin{cases} \left(1 - \frac{\delta_{(2m)n}}{2}\right)\left[\tilde{\theta}^2_{m\Omega}\frac{d\theta^2_{(n-m)\Omega}}{d\tilde{\theta}_{n\Omega}} + \tilde{\theta}^2_{(n-m)\Omega}\frac{d\theta^2_{m\Omega}}{d\tilde{\theta}_{n\Omega}}\right] \\ \quad (\text{if } n \geqslant 2m) \\ + \\ \left(1 - \frac{\delta_{0n}}{2}\right)\left[\tilde{\theta}^{2*}_{m\Omega}\frac{d\theta^2_{(n+m)\Omega}}{d\tilde{\theta}_{n\Omega}} + \tilde{\theta}^2_{(n+m)\Omega}\frac{d\theta^{2*}_{m\Omega}}{d\tilde{\theta}_{n\Omega}}\right] \\ \quad (\text{if } n+m \leqslant 2N) \end{cases} \quad (18a)$$

$$\frac{d\theta^2_{k\Omega}}{d\tilde{\theta}_{n\Omega}} = \begin{cases} \tilde{\theta}_{(k-n)\Omega} & (\text{if } k \geqslant n) \\ + & \\ (1 - \delta_{0k}/2)\tilde{\theta}^*_{(n-k)\Omega} & (\text{if } k \leqslant n) \\ + & \\ (1 - \delta_{0k}/2)\tilde{\theta}_{(k+n)\Omega} & (\text{if } k+n \leqslant N) \end{cases}. \quad (18b)$$

The system of equations (12) is solved numerically for a discretized domain of 200 nodes. The integral in Eq. (9) can be evaluated numerically by Gaussian integration. Since the solution is obtained iteratively, convergence will depend on the quality of the initial guess at the temperature distribution through the plane-wall. Generally, the initial guess is that the steady and 1Ω temperature components vary linearly through the plane-wall between their respective boundary values and higher frequency components are all zero.

4. Results

To validate the numerical implementation of this method, a test case is considered in which an optically thin plane-wall is heated by blackbody radiation from the fluid at a nonconstant temperature θ_a adjacent to the front surface. No conduction of heat occurs between the front surface of the plane-wall and the fluid, $q_c = 0$. The back surface of the plane-wall and the adjacent fluid are held at zero temperature $\theta(\eta = 1) = \theta_b = 0$. In the optically thin limit, the radiation term, Eq. (3b), becomes:

$$S|_{\lambda\to 0} = -\frac{\theta^4_a}{2}. \quad (19)$$

Notice that in this limit, radiative heating becomes uniform and emission becomes negligible inside the plane-wall.

A solution to the problem stated is sought through an expansion of temperature with $N = 4$ frequencies. An exact solution exists because radiation transfer no longer depends on emission from within the plane-wall (for $n > 4$, $\widetilde{S}_{n\Omega} = 0$). For each component of the temperature field, an analytic solution to Eq. (6) is found subject to the boundary condition equations. (10a) and (10d)

$$\bar{\theta}_0 = \frac{\lambda\bar{\theta}^4_{a,0}}{4\kappa}(1 - \eta^2), \quad (20a)$$

$$\tilde{\theta}_{n\Omega} = \frac{i\lambda}{2\Omega}\frac{\tilde{\theta}^4_{a,n\Omega}}{n}\left[\frac{\cosh(\eta\sqrt{in\Omega/\kappa})}{\cosh(\sqrt{in\Omega/\kappa})} - 1\right]. \quad (20b)$$

From Eqs. (20a,b), the final solution is constructed using Eq. (5) with $N = 4$.

For the test problem, the fluid adjacent to the front surface has a steady and a 1Ω temperature component of equal unit amplitude, $\bar{\theta}_{a,0} = \tilde{\theta}_{a,\Omega} = 1$. For this, the expanded terms for θ^4_a used in Eqs. (20a,b) are $\bar{\theta}^4_{a,0} = 35/8$, $\tilde{\theta}^4_{a,\Omega} = 7$, $\tilde{\theta}^4_{a,2\Omega} = 7/2$, $\tilde{\theta}^4_{a,3\Omega} = 1$ and $\tilde{\theta}^4_{a,4\Omega} = 1/8$ (using Eqs. (7) and (8)). Taking the fundamental frequency to be $\Omega = 1$ and the conduction–radiation parameter to be $\kappa = 1$, the analytic solution is compared with a numerical solution using $N = 16$ temperature frequencies. Fig. 2 shows the amplitude of the first five temperature components as a function of optical thickness for both the numerical and analytic solutions. For an optical thickness less than $\lambda = 0.01$ the numerical results are indistinguishable from the analytical result given by Eqs. (20a,b). The agreement worsens as the optical thickness increases, because the validity of the analytical result begins to fail. The test problem demonstrates that in the optically thin limit, the numerical results are correct. This validates the numerical implementation of the complex combination solution for conduction transport with spatially uniform radiative heating. However, the implementation of radiative emission and absorption of radiation originating from locations within the plane-wall has yet to be tested.

To validate calculations of emission and re-absorption of radiation in the medium, a second test case is considered in which the steady temperature distribution across the plane-wall is found. Both front and back surface temperatures are fixed at the fluid temperatures $\theta(\eta = 0) = \theta_a$ and $\theta(\eta = 1) = \theta_b$. Conduction and blackbody radiation of heat is exchanged between the plane-wall and both fluids. Although the fluid temperatures are steady, this problem can only be solved numerically. For comparison with the results found in [16], the fluid temperatures are set as $\theta_a = 1.0$ and $\theta_b = 0.1$, and the optical thickness as $\lambda = 1$. Eq. (6) is solved for the steady solution subject to the boundary conditions of Eqs. (10b) and (10d). Fig. 3 shows the numerical results over a wide range of the conduction–radiation parameter κ. In the limit that $\kappa \to \infty$, the temperature distribution becomes linear between the two boundary temperatures. In this limit, radiation transport is negligible and the solution for simple conduction transport is revealed. The more interesting cases arise when the conduction–radiation parameter becomes small, making radiation transport significant. For very small values of κ, temperature "slip" is observed in the solution at the boundaries. Over the entire range of κ, the results shown in Fig. 3 are in agreement with those reported in [16]. This validates the numerical implementation of steady radiation–conduction transfer of heat through the plane-wall.

To study the complex combination method for a more general case, a problem is considered in which no

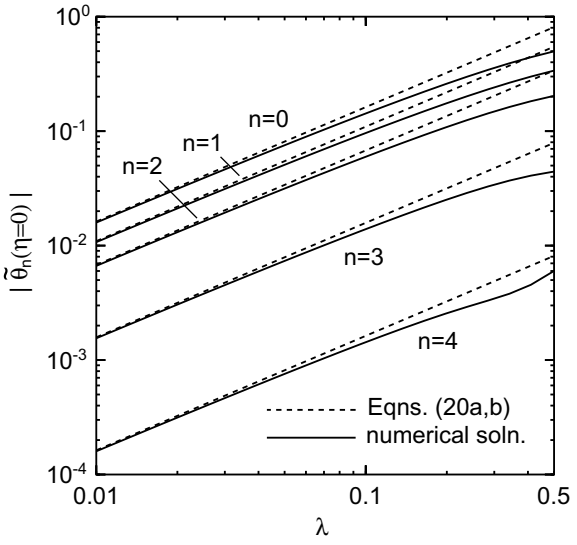

Fig. 2. Comparison of analytic solution valid in the limit of an optically thin plane-wall with numerical results. The first five temperature components are shown as a function of optical thickness.

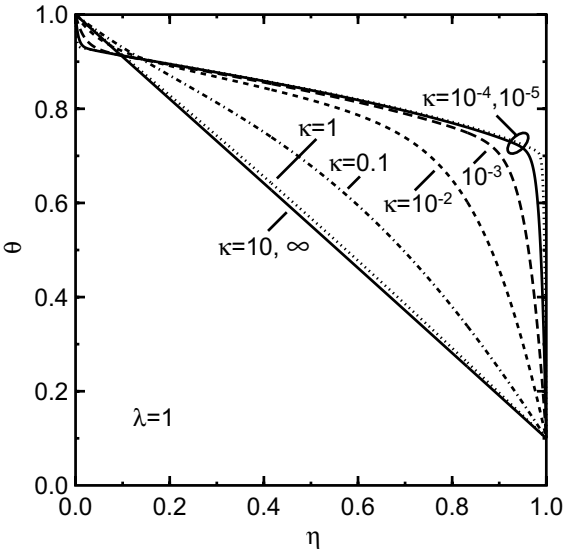

Fig. 3. The steady temperature distribution across the plane-wall with an optical thickness $\lambda = 1$ and fixed surface temperatures. Results are shown over a wide range of the conduction–radiation parameter κ.

radiation enters the plane-wall from either boundary, but originates from emission within the wall. Convection with $Nu = 1$ occurs from the back surface to fluid with zero temperature. A conduction heat flux is imposed on the front surface that has a steady and a 1Ω component of equal amplitude, $\overline{Q}_0 = \widetilde{Q}_\Omega = 1$. The fundamental frequency is $\Omega = 1$, the conduction–radiation parameter is $\kappa = 1$, and the optical thickness of the plane-wall is $\lambda = 1$.

A solution is sought using an expansion of temperature with 16 frequencies. Fig. 4 shows the solution in terms of the amplitude of different frequency components as they vary spatially across the plane-wall. The steady component has the largest amplitude, and each component thereafter decreases in amplitude with increasing frequency. By a frequency of 7Ω, the temperature amplitude is 10^{-4} of that at the fundamental frequency, indicating that higher frequencies are not needed. As $\eta \to 0$, the slopes in temperature approach unity for the steady and the 1Ω fields, as imposed by the boundary condition. In contrast, at the same boundary, the slopes in temperature of the 2Ω and higher frequencies are zero, which is also imposed by the boundary condition.

Unlike a pure conduction problem, the spatial variation of the steady temperature field shown in Fig. 4 is nonlinear because of the change in relative contribution of conduction and radiation to transport over the thickness of the plane-wall. Due to the heat capacity of the material, the amplitude of the transient components of the solution decay more rapidly with distance from the heat source than the steady solution. However, radiation transfer increases the thermal penetration depth relative to conduction alone.

The complex temperature components can be put back into the time domain using Eq. (5). In Fig. 5, the temporal response at the back surface is shown as a function of time for a few frequency components individually, then as a complete solution. Again the temperature amplitude of individual frequency components decays with increasing frequency, as shown in Fig. 5(a). The complete solution shown in Fig. 5(b) is constructed by superposition of the individual frequency components using Eq. (5). It is interesting to note that the elevated temperature broadens as a result of mixed radiation–conduction transport having two different timescales. In contrast, a process of diffusion by conduction alone would be symmetric about the mean temperature value.

In Fig. 6, the back surface temperature is analyzed for temporal changes resulting from the number of frequencies used in the solution. As the number of temperature frequencies N representing the solution goes to infinity, the truncated radiation terms in Eq. (6) should become negligible. In going from an approximate harmonic solution with $N = 1$ to an approximate solution with $N = 2$ there is a marked shift in phase. With as few as $N = 3$ temperature frequencies the solution becomes indistinguishable in the figure from that with $N \to \infty$. It should be noted that although the solution with $N = 1$ is

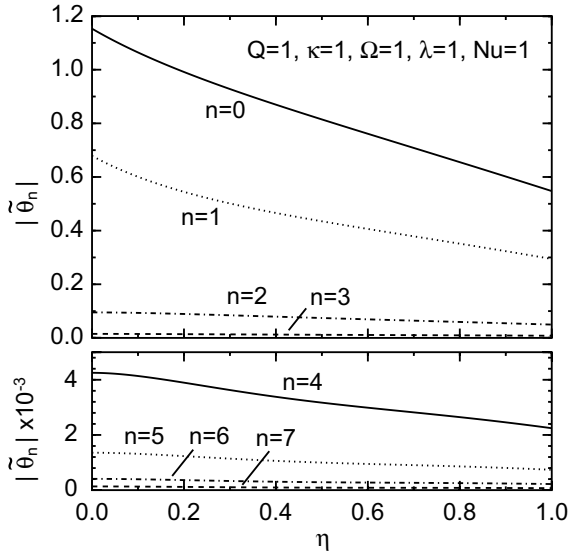

Fig. 4. Amplitude variation across the plane-wall of the first eight temperature frequency components. A harmonic conduction heat flux is imposed on the front surface $\overline{Q}_0 = \widetilde{Q}_\Omega = 1$, and convection occurs from the back surface to fluid with zero temperature.

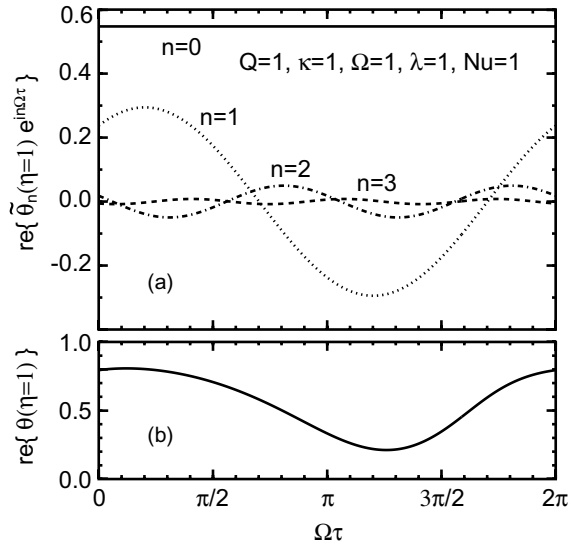

Fig. 5. Solution in the time domain at the back surface for same problem conditions as in Fig. 4. Solution is shown in (a) as a function of time for a few frequency components individually, then in (b) as a complete solution.

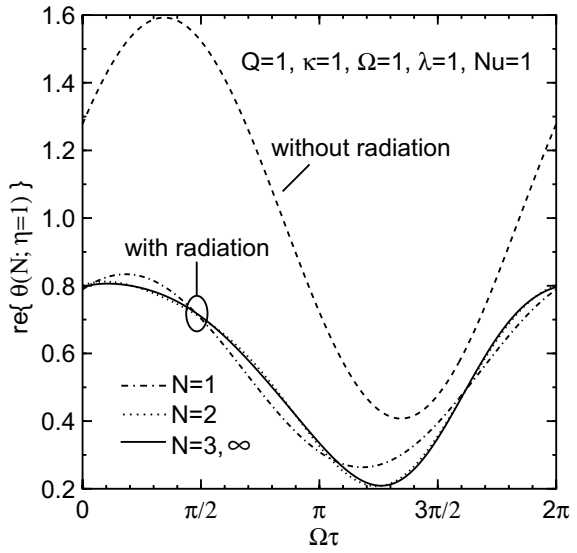

Fig. 6. The back surface conduction–radiation solution analyzed for temporal changes resulting from the number of temperature frequencies used. Also shown is the conduction solution without radiation transport. The problem conditions are the same as in Figs. 4 and 5.

harmonic, it still contains an approximate contribution of radiation transport, and is not equivalent to the harmonic solution obtained from diffusion by conduction alone. To illustrate this, Fig. 6 also contains the analytic solution of the same problem without radiation transport. For pure conduction, the nonzero temperature coefficients of Eq. (5) that describe the solution at the back surface are

$$\bar{\theta}_0(\eta=1)=\frac{\bar{Q}_0}{\kappa Nu}, \tag{21a}$$

$$\tilde{\theta}_\Omega(\eta=1)=\frac{\tilde{Q}_\Omega/\kappa}{Nu\cdot\cosh(\sqrt{\mathrm{i}\Omega/\kappa})+\sqrt{\mathrm{i}\Omega/\kappa}\cdot\sinh(\sqrt{\mathrm{i}\Omega/\kappa})}. \tag{21b}$$

With radiation, the overall temperature in the plane-wall is lower than without due to radiative loss of energy. Additionally, the back surface temperature maximum occurs much earlier with radiation than without.

In general, the percent error in the approximated solution $\theta(N;\eta,\Omega\tau)$ constructed from N temperature frequencies depends upon the position and time at which the solution is evaluated. An average percent error in the solution can be defined as

$$\langle\theta_{\mathrm{err}}(N)\rangle=100\times\int_0^{2\pi}\frac{\mathrm{d}(\Omega\tau)}{2\pi}\times\int_0^1\mathrm{d}\eta\left|\frac{\mathrm{re}\{\theta(N;\eta,\Omega\tau)\}}{\mathrm{re}\{\theta(\infty;\eta,\Omega\tau)\}}-1\right|, \tag{22}$$

where $\theta(\infty;\eta,\Omega\tau)$ is the solution for $N\to\infty$. Fig. 7 shows the average percent error in the solution as a function of the number of temperature frequencies used. Eq. (22) is evaluated with $N\to\infty$ represented by $N=32$. Fig. 7 illustrates that the size of N required for an acceptably accurate solution depends on the value of the conduction–radiation parameter κ, the optical thickness of the plane-wall λ, and the fundamental frequency of the heating source Ω. In this figure, only one parameter is varied from unity at a time.

One expects that for a large value of the conduction–radiation parameter κ, the solution will reflect well a harmonic conduction problem that can be obtained with $N=1$. For $\kappa=10$, Fig. 7(a) shows that the average percent error in the solution for $N=1$ is less than 1%. For $1\geqslant\kappa\geqslant0.1$, $N=3$ is required for comparably accurate solutions. Over this range of κ, the solution dependence on N remains relatively similar.

The optical thickness has an interesting effect on the solution. As $\lambda\to0$ both emission and re-absorption of radiation go to zero. In this limit, transport is dominated by conduction and the solution becomes harmonic. This trend is seen in Fig. 7(b). For $1\leqslant\lambda\leqslant10$ the solution dependence on N remains relatively similar, and the number of temperature frequencies required to obtain an average error less than 1% is $N=3$.

It was seen that temperature components in the solution decrease in amplitude with increasing frequency. Furthermore, increasing the fundamental frequency Ω will increase all the expansion frequencies. As a consequence, the required number of temperature frequencies used in the solution will decrease as the fundamental frequency increases. This trend is shown in Fig. 7(c). For $\Omega=10$ the solution is virtually harmonic with the average error being just above 0.1% when $N=1$. However, when $\Omega=0.1$ the number of temperature frequencies required to obtain an average error less than 0.1% is $N=10$. The cumulative information in Fig. 7 reveals that with as few as $N=4$ temperature frequencies, satisfactory solutions can be obtained if the fundamental frequency is $\Omega\geqslant1$ irrespective of the conduction–radiation parameter κ and the optical thickness λ of the plane-wall.

Until this point it has been assumed that all boundary conditions are harmonic. However, this is not a constraint of the complex combination solution method. In general any arbitrary periodic function, represented as a Fourier expansion, can be applied as one or more of the boundary conditions without changing the current formulation. Consider another problem in which no radiation enters the plane-wall from the boundaries, and convection with $Nu=1$ occurs from the back surface to fluid with zero temperature. Although the front fluid temperature is set to zero to eliminate radiation, a sawtooth temperature boundary condition is applied to the front surface having an amplitude that varies between 0

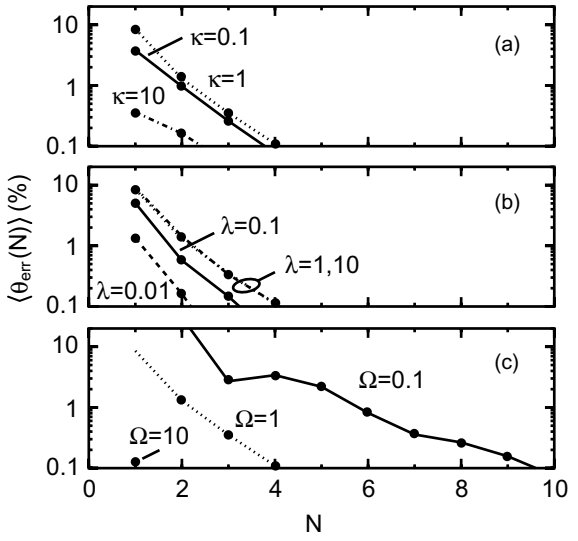

Fig. 7. The average percent error in the solution as a function of the number of temperature frequencies used. The problem conditions are the same as in Figs. 4–6, with variation in each panel of: (a) the conduction–radiation parameter, κ; (b) the optical thickness of the plane-wall λ and (c) the fundamental frequency of the heat flux boundary condition Ω.

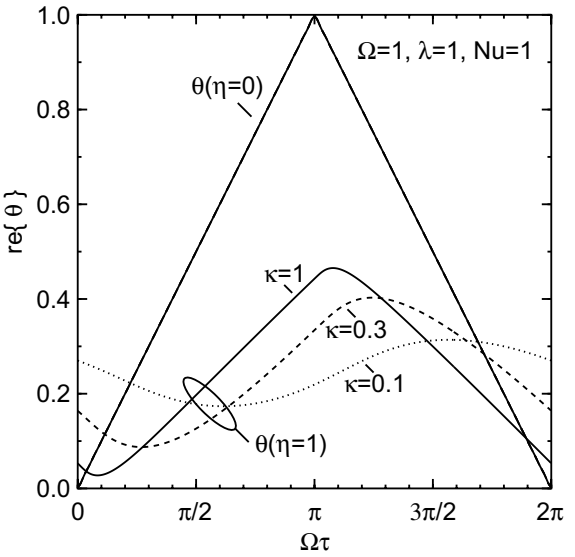

Fig. 8. The time dependence of temperature at the front and back surfaces of a plane-wall experiencing a saw-tooth temperature boundary condition. Convection occurs from the back surface to fluid with zero temperature. Results are shown for three values of the conduction–radiation parameter, κ.

and 1, with a period of $\Omega = 1$. This function is represented in the form of Eq. (5) with $N \to \infty$ and constant coefficients given by

$$\bar{\theta}_{a,0} = \frac{1}{2}, \tilde{\theta}_{a,n\Omega} = \begin{cases} -4/(n\pi)^2, & \text{odd } n, \\ 0, & \text{even } n. \end{cases} \quad (23a,b)$$

A reasonable representation of the saw-tooth function requires only a finite number of terms, since this series converges reasonably fast. If a sufficiently large number of terms are used to express the boundary condition, it is not necessary to expand further the number of terms for the temperature solution in the plane-wall (as is generally the case due to the multiplicative effect of radiation).

A solution is sought for the temperature distribution in the plane-wall with optical thickness $\lambda = 1$ using an $N = 50$ frequency expansion of temperature. The large number of frequencies used is for good temporal definition near the saw-tooth temperature boundary condition. Fig. 8 shows the time dependence of temperature at the front and back surfaces of the plane-wall for different values of the conduction–radiation parameter κ. At the front surface, temperature follows the specified saw-tooth temperature boundary condition. However, at the back surface two points are observed. First, there is a phase delay in the back surface temperature that results from the finite time required for conduction and radiation to transport energy through the plane-wall. This phase delay grows longer as transport is inhibited by reducing the conduction–radiation parameter κ, which is accompanied by a reduction in amplitude. Second, the temporal definition of the saw-tooth shape at the back surface degrades as κ is reduced. Although diffusion by conduction alone degrades the saw-tooth shape as one moves away from the front boundary, the second observation illustrates that radiation can accelerate this effect.

Recall that in Fig. 6 the temperature at the back surface is advanced in phase by the contribution of radiation to the overall transport of energy. This makes sense since radiation enhances the penetration of heat into the plane-wall over conduction transport alone. However, in Fig. 8 it is observed that the phase of the temperature field at the back surface is retarded as a consequence of the conduction–radiation parameter κ decreasing (radiation transport becoming more dominate). The explanation for this is found in the decomposed temperature field. When κ decreases, the 1Ω temperature frequency amplitude decreases because of a loss of conduction transport. However, the 2Ω temperature frequency increases because it originates through the absorption of emission originating from within the plane-wall, which is a process that strengthens as κ decreases. Consulting Fig. 5, it is seen that if the 1Ω temperature frequency amplitude decreases as the 2Ω

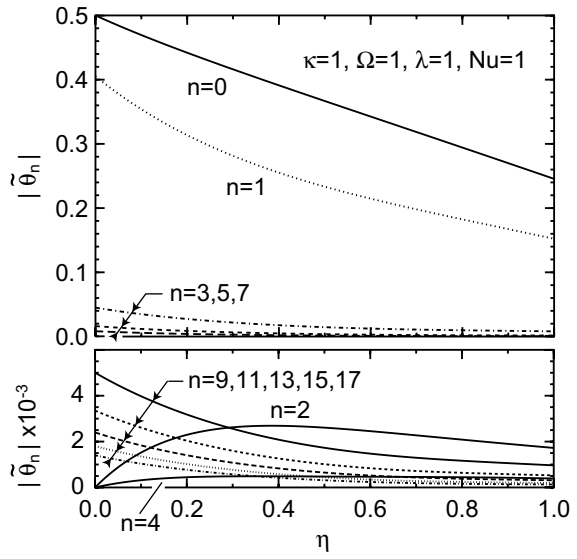

Fig. 9. The solution for the saw-tooth boundary condition problem in terms of the amplitude of different frequency components as they vary spatially across the plane-wall. The problem conditions are the same as in Fig. 8.

temperature frequency increases, the phase of the complete temperature will shift back in time.

Fig. 9 shows the solution for the saw-tooth boundary condition problem in terms of the amplitude of different frequency components as they vary spatially across the plane-wall. The relatively strong components to the solution are the steady and odd frequencies of 1Ω, 3Ω, 5Ω, and 7Ω. Even frequencies in this solution are weak due to their absence in the boundary condition, and exist only because of the nonlinear radiative coupling of energy into these frequencies. The strongest even frequency is 2Ω, with an amplitude of comparable importance to 9Ω in the odd frequencies sequence. The even frequencies and the odd frequencies below 7Ω individually contribute amplitudes of the order of 0.1% of the full solution. Near the surface, the high odd frequency components constructively conspire to give good temporal definition to the saw-tooth temperature boundary condition. However, away from the surface, the temperature components in the lower panel of Fig. 9 offer little to the total solution.

5. Summary

A mixed-mode model for radiation and conduction transport has been developed using complex combination to solve problems with periodic boundary conditions. Implementation of the model was verified by comparisons with an analytic solution valid for a plane-wall in the optically thin limit, and with previously established steady-state numerical solutions for a plane-wall with greater opacity. Solutions were expressed as an expansion series of temperature fields having frequencies that are multiples of those imposed by the boundary conditions. These solutions were shown to converge with as few as $N = 4$ temperature frequencies when the fundamental frequency $\Omega = \rho CL\omega/(4\mathbb{m}^2\sigma T_r^3)$ is of order unity or greater. The generality of the method was then illustrated by considering a problem having a non-harmonic boundary condition. This demonstrated the relative ease with which the complex combination method can be used to analyze any mixed radiation–conduction transport problem with cyclic thermal loading.

Acknowledgements

This work was supported by the National Science Foundation under Grants No. CTS-9875860 and DMR-0099695.

References

[1] C.-F. Tsai, G. Nixon, Transient temperature distribution of a multilayer composite wall with effects of internal thermal radiation and conduction, Numer. Heat Transfer 10 (1) (1986) 95–101.
[2] C.C. Lii, M.N. Ozisik, Transient radiation and conduction in an absorbing, emitting, scattering slab with reflective boundaries, Int. J. Heat Mass Transfer 15 (5) (1972) 1175–1179.
[3] T. Chung-Jen, C. Hsin-Sen, Transient combined conduction and radiation in an absorbing, emitting and anisotropically-scattering medium with variable thermal conductivity, Int. J. Heat Mass Transfer 35 (7) (1992) 1844–1847.
[4] I. Anteby, I. Shai, A. Arbel, Numerical calculations for combined conduction and radiation transient heat transfer in a semitransparent medium, Numer. Heat Transfer, Part A 37 (4) (2000) 359–371.
[5] T. Morel, S. Wahiduzzaman, Effect of translucence of engineering ceramics on heat transfer in diesel engines, Oak Ridge National Laboratory Report ORNL/Sub/88-22042/2, Oak Ridge, TN, 1992.
[6] R. Siegel, C.M. Spuckler, Analysis of thermal radiation effects on temperatures in turbine engine thermal barrier coatings, Mater. Sci. Eng. A A245 (2) (1998) 150–159.
[7] D.L. Wood, K. Nassau, Refractive index of cubic zirconia stabilized with yttria, Appl. Opt. 21 (16) (1982) 2978–2981.
[8] R.C. Buchanan, S. Pope, Optical and electrical properties of yttria stabilized zirconia (YSZ) crystals, J. Electrochem. Soc. 130 (4) (1983) 962–966.
[9] D.R. Clarke, Materials selection guidelines for low thermal conductivity thermal barrier coatings, Surface Coating Technol. (in press).

[10] S. Gu, T.J. Lu, D.D. Hass, H.N.G. Wadley, Thermal conductivity of zirconia coatings with zig-zag pore microstructures, Acta Mater. 49 (13) (2001) 2539–2547.
[11] P. Scardi, M. Leoni, Microstructure and heat transfer phenomena in ceramic thermal barrier coatings, J. Am. Ceram. Soc. 84 (4) (2001) 827–835.
[12] L. Tian Jian, C.G. Levi, H.N.G. Wadley, A.G. Evans, Distributed porosity as a control parameter for oxide thermal barriers made by physical vapor deposition, J. Am. Ceram. Soc. 84 (12) (2001) 2937–2946.
[13] P.G. Klemens, M. Gell, Thermal conductivity of thermal barrier coatings, Mater. Sci. Eng. A A245 (2) (1998) 143–149.
[14] G.E. Myers, Analytical methods in conduction heat transfer, second ed., AMCHT Publications, Madison, WI, 1998.
[15] R. Siegel, J.R. Howell, Thermal radiation heat transfer, fourth ed., Taylor & Francis, New York, 2002.
[16] R. Viskanta, R.J. Grosh, Heat transfer by simultaneous conduction and radiation in absorbing medium, J. Heat Transfer 84 (1) (1962) 63–72.